Measurement of $\mathcal{B}(t \to Wb)/\mathcal{B}(t \to Wq)$ at the Collider Detector at Fermilab

D. Acosta,[16] J. Adelman,[12] T. Affolder,[9] T. Akimoto,[54] M.G. Albrow,[15] D. Ambrose,[15] S. Amerio,[42] D. Amidei,[33] A. Anastassov,[50] K. Anikeev,[15] A. Annovi,[44] J. Antos,[1] M. Aoki,[54] G. Apollinari,[15] T. Arisawa,[56] J-F. Arguin,[32] A. Artikov,[13] W. Ashmanskas,[15] A. Attal,[7] F. Azfar,[41] P. Azzi-Bacchetta,[42] N. Bacchetta,[42] H. Bachacou,[28] W. Badgett,[15] A. Barbaro-Galtieri,[28] G.J. Barker,[25] V.E. Barnes,[46] B.A. Barnett,[24] S. Baroiant,[6] G. Bauer,[31] F. Bedeschi,[44] S. Behari,[24] S. Belforte,[53] G. Bellettini,[44] J. Bellinger,[58] A. Belloni,[31] E. Ben-Haim,[15] D. Benjamin,[14] A. Beretvas,[15] T. Berry,[29] A. Bhatti,[48] M. Binkley,[15] D. Bisello,[42] M. Bishai,[15] R.E. Blair,[2] C. Blocker,[5] K. Bloom,[33] B. Blumenfeld,[24] A. Bocci,[48] A. Bodek,[47] G. Bolla,[46] A. Bolshov,[31] D. Bortoletto,[46] J. Boudreau,[45] S. Bourov,[15] B. Brau,[9] C. Bromberg,[34] E. Brubaker,[12] J. Budagov,[13] H.S. Budd,[47] K. Burkett,[15] G. Busetto,[42] P. Bussey,[19] K.L. Byrum,[2] S. Cabrera,[14] M. Campanelli,[18] M. Campbell,[33] F. Canelli,[7] A. Canepa,[46] M. Casarsa,[53] D. Carlsmith,[58] R. Carosi,[44] S. Carron,[14] M. Cavalli-Sforza,[3] A. Castro,[4] P. Catastini,[44] D. Cauz,[53] A. Cerri,[28] L. Cerrito,[41] J. Chapman,[33] Y.C. Chen,[1] M. Chertok,[6] G. Chiarelli,[44] G. Chlachidze,[13] F. Chlebana,[15] I. Cho,[27] K. Cho,[27] D. Chokheli,[13] J.P. Chou,[20] S. Chuang,[58] K. Chung,[11] W-H. Chung,[58] Y.S. Chung,[47] M. Cijliak,[44] C.I. Ciobanu,[23] M.A. Ciocci,[44] A.G. Clark,[18] D. Clark,[5] M. Coca,[14] A. Connolly,[28] M. Convery,[48] J. Conway,[6] B. Cooper,[30] K. Copic,[33] M. Cordelli,[17] G. Cortiana,[42] J. Cranshaw,[52] J. Cuevas,[10] A. Cruz,[16] R. Culbertson,[15] C. Currat,[28] D. Cyr,[58] D. Dagenhart,[5] S. Da Ronco,[42] S. D'Auria,[19] P. de Barbaro,[47] S. De Cecco,[49] A. Deisher,[28] G. De Lentdecker,[47] M. Dell'Orso,[44] S. Demers,[47] L. Demortier,[48] M. Deninno,[4] D. De Pedis,[49] P.F. Derwent,[15] C. Dionisi,[49] J.R. Dittmann,[15] P. DiTuro,[50] C. Dörr,[25] A. Dominguez,[28] S. Donati,[44] M. Donega,[18] J. Donini,[42] M. D'Onofrio,[18] T. Dorigo,[42] K. Ebina,[56] J. Efron,[38] J. Ehlers,[18] R. Erbacher,[6] M. Erdmann,[25] D. Errede,[23] S. Errede,[23] R. Eusebi,[47] H-C. Fang,[28] S. Farrington,[29] I. Fedorko,[44] W.T. Fedorko,[12] R.G. Feild,[59] M. Feindt,[25] J.P. Fernandez,[46] R.D. Field,[16] G. Flanagan,[34] L.R. Flores-Castillo,[45] A. Foland,[20] S. Forrester,[6] G.W. Foster,[15] M. Franklin,[20] J.C. Freeman,[28] Y. Fujii,[26] I. Furic,[12] A. Gajjar,[29] M. Gallinaro,[48] J. Galyardt,[11] M. Garcia-Sciveres,[28] A.F. Garfinkel,[46] C. Gay,[59] H. Gerberich,[14] D.W. Gerdes,[33] E. Gerchtein,[11] S. Giagu,[49] P. Giannetti,[44] A. Gibson,[28] K. Gibson,[11] C. Ginsburg,[15] K. Giolo,[46] M. Giordani,[53] M. Giunta,[44] G. Giurgiu,[11] V. Glagolev,[13] D. Glenzinski,[15] M. Gold,[36] N. Goldschmidt,[33] D. Goldstein,[7] J. Goldstein,[41] G. Gomez,[10] G. Gomez-Ceballos,[10] M. Goncharov,[51] O. González,[46] I. Gorelov,[36] A.T. Goshaw,[14] Y. Gotra,[45] K. Goulianos,[48] A. Gresele,[42] M. Griffiths,[29] C. Grosso-Pilcher,[12] U. Grundler,[23] J. Guimaraes da Costa,[20] C. Haber,[28] K. Hahn,[43] S.R. Hahn,[15] E. Halkiadakis,[47] A. Hamilton,[32] B-Y. Han,[47] R. Handler,[58] F. Happacher,[17] K. Hara,[54] M. Hare,[55] R.F. Harr,[57] R.M. Harris,[15] F. Hartmann,[25] K. Hatakeyama,[48] J. Hauser,[7] C. Hays,[14] H. Hayward,[29] B. Heinemann,[29] J. Heinrich,[43] M. Hennecke,[25] M. Herndon,[24] C. Hill,[9] D. Hirschbuehl,[25] A. Hocker,[15] K.D. Hoffman,[12] A. Holloway,[20] S. Hou,[1] M.A. Houlden,[29] B.T. Huffman,[41] Y. Huang,[14] R.E. Hughes,[38] J. Huston,[34] K. Ikado,[56] J. Incandela,[9] G. Introzzi,[44] M. Iori,[49] Y. Ishizawa,[54] C. Issever,[9] A. Ivanov,[6] Y. Iwata,[22] B. Iyutin,[31] E. James,[15] D. Jang,[50] B. Jayatilaka,[33] D. Jeans,[49] H. Jensen,[15] E.J. Jeon,[27] M. Jones,[46] K.K. Joo,[27] S.Y. Jun,[11] T. Junk,[23] T. Kamon,[51] J. Kang,[33] M. Karagoz Unel,[37] P.E. Karchin,[57] Y. Kato,[40] Y. Kemp,[25] R. Kephart,[15] U. Kerzel,[25] V. Khotilovich,[51] B. Kilminster,[38] D.H. Kim,[27] H.S. Kim,[23] J.E. Kim,[27] M.J. Kim,[11] M.S. Kim,[27] S.B. Kim,[27] S.H. Kim,[54] Y.K. Kim,[12] M. Kirby,[14] L. Kirsch,[5] S. Klimenko,[16] M. Klute,[31] B. Knuteson,[31] B.R. Ko,[14] H. Kobayashi,[54] D.J. Kong,[27] K. Kondo,[56] J. Konigsberg,[16] K. Kordas,[32] A. Korn,[31] A. Korytov,[16] A.V. Kotwal,[14] A. Kovalev,[43] J. Kraus,[23] I. Kravchenko,[31] A. Kreymer,[15] J. Kroll,[43] M. Kruse,[14] V. Krutelyov,[51] S.E. Kuhlmann,[2] S. Kwang,[12] A.T. Laasanen,[46] S. Lai,[32] S. Lami,[44] S. Lammel,[15] M. Lancaster,[30] R. Lander,[6] K. Lannon,[38] A. Lath,[50] G. Latino,[44] I. Lazzizzera,[42] C. Lecci,[25] T. LeCompte,[2] J. Lee,[27] J. Lee,[47] S.W. Lee,[51] R. Lefèvre,[3] N. Leonardo,[31] S. Leone,[44] S. Levy,[12] J.D. Lewis,[15] K. Li,[59] C. Lin,[59] C.S. Lin,[15] M. Lindgren,[15] E. Lipeles,[8] T.M. Liss,[23] A. Lister,[18] D.O. Litvintsev,[15] T. Liu,[15] Y. Liu,[18] N.S. Lockyer,[43] A. Loginov,[35] M. Loreti,[42] P. Loverre,[49] R-S. Lu,[1] D. Lucchesi,[42] P. Lujan,[28] P. Lukens,[15] G. Lungu,[16] L. Lyons,[41] J. Lys,[28] R. Lysak,[1] E. Lytken,[46] D. MacQueen,[32] R. Madrak,[15] K. Maeshima,[15] P. Maksimovic,[24] G. Manca,[29] Margaroli,[4] R. Marginean,[15] C. Marino,[23] A. Martin,[59] M. Martin,[24] V. Martin,[37] M. Martínez,[3] T. Maruyama,[54] H. Matsunaga,[54] M. Mattson,[57] P. Mazzanti,[4] K.S. McFarland,[47] D. McGivern,[30] P.M. McIntyre,[51] P. McNamara,[50] McNulty,[29] A. Mehta,[29] S. Menzemer,[31] A. Menzione,[44] P. Merkel,[46] C. Mesropian,[48] A. Messina,[49] T. Miao,[15] N. Miladinovic,[5] J. Miles,[31] L. Miller,[20] R. Miller,[34] J.S. Miller,[33] C. Mills,[9] R. Miquel,[28] S. Miscetti,[17] G. Mitselmakher,[16] A. Miyamoto,[26] N. Moggi,[4] B. Mohr,[7] R. Moore,[15] M. Morello,[44] P.A. Movilla Fernandez,[28] J. Muelmenstaedt,[28] A. Mukherjee,[15] M. Mulhearn,[31] T. Muller,[25] R. Mumford,[24] A. Munar,[43] P. Murat,[15] J. Nachtman,[15] S. Nahn,[59] I. Nakano,[39] A. Napier,[55] R. Napora,[24]

D. Naumov,[36] V. Necula,[16] T. Nelson,[15] C. Neu,[43] M.S. Neubauer,[8] J. Nielsen,[28] T. Nigmanov,[45] L. Nodulman,[2] O. Norniella,[3] T. Ogawa,[56] S.H. Oh,[14] Y.D. Oh,[27] T. Ohsugi,[22] T. Okusawa,[40] R. Oldeman,[29] R. Orava,[21] W. Orejudos,[28] K. Osterberg,[21] C. Pagliarone,[44] E. Palencia,[10] R. Paoletti,[44] V. Papadimitriou,[15] A.A. Paramonov,[12] S. Pashapour,[32] J. Patrick,[15] G. Pauletta,[53] M. Paulini,[11] C. Paus,[31] D. Pellett,[6] A. Penzo,[53] T.J. Phillips,[14] G. Piacentino,[44] J. Piedra,[10] K.T. Pitts,[23] C. Plager,[7] L. Pondrom,[58] G. Pope,[45] X. Portell,[3] O. Poukhov,[13] N. Pounder,[41] F. Prakoshyn,[13] A. Pronko,[16] J. Proudfoot,[2] F. Ptohos,[17] G. Punzi,[44] J. Rademacker,[41] M.A. Rahaman,[45] A. Rakitine,[31] S. Rappoccio,[20] F. Ratnikov,[50] H. Ray,[33] B. Reisert,[15] V. Rekovic,[36] P. Renton,[41] M. Rescigno,[49] F. Rimondi,[4] K. Rinnert,[25] L. Ristori,[44] W.J. Robertson,[14] A. Robson,[19] T. Rodrigo,[10] S. Rolli,[55] R. Roser,[15] R. Rossin,[16] C. Rott,[46] J. Russ,[11] V. Rusu,[12] A. Ruiz,[10] D. Ryan,[55] H. Saarikko,[21] S. Sabik,[32] A. Safonov,[6] R. St. Denis,[19] W.K. Sakumoto,[47] G. Salamanna,[49] D. Saltzberg,[7] C. Sanchez,[3] L. Santi,[53] S. Sarkar,[49] K. Sato,[54] P. Savard,[32] A. Savoy-Navarro,[15] P. Schlabach,[15] E.E. Schmidt,[15] M.P. Schmidt,[59] M. Schmitt,[37] T. Schwarz,[33] L. Scodellaro,[10] A.L. Scott,[9] A. Scribano,[44] F. Scuri,[44] A. Sedov,[46] S. Seidel,[36] Y. Seiya,[40] A. Semenov,[13] F. Semeria,[4] L. Sexton-Kennedy,[15] I. Sfiligoi,[17] M.D. Shapiro,[28] T. Shears,[29] P.F. Shepard,[45] D. Sherman,[20] M. Shimojima,[54] M. Shochet,[12] Y. Shon,[58] I. Shreyber,[35] A. Sidoti,[44] A. Sill,[52] P. Sinervo,[32] A. Sisakyan,[13] J. Sjolin,[41] A. Skiba,[25] A.J. Slaughter,[15] K. Sliwa,[55] D. Smirnov,[36] J.R. Smith,[6] F.D. Snider,[15] R. Snihur,[32] M. Soderberg,[33] A. Soha,[6] S.V. Somalwar,[50] J. Spalding,[15] M. Spezziga,[52] F. Spinella,[44] P. Squillacioti,[44] H. Stadie,[25] M. Stanitzki,[59] B. Stelzer,[32] O. Stelzer-Chilton,[32] D. Stentz,[37] J. Strologas,[36] D. Stuart,[9] J. S. Suh,[27] A. Sukhanov,[16] K. Sumorok,[31] H. Sun,[55] T. Suzuki,[54] A. Taffard,[23] R. Tafirout,[32] H. Takano,[54] R. Takashima,[39] Y. Takeuchi,[54] K. Takikawa,[54] M. Tanaka,[2] R. Tanaka,[39] N. Tanimoto,[39] M. Tecchio,[33] P.K. Teng,[1] K. Terashi,[48] R.J. Tesarek,[15] S. Tether,[31] J. Thom,[15] A.S. Thompson,[19] E. Thomson,[43] P. Tipton,[47] V. Tiwari,[11] S. Tkaczyk,[15] D. Toback,[51] K. Tollefson,[34] T. Tomura,[54] D. Tonelli,[44] M. Tönnesmann,[34] S. Torre,[44] D. Torretta,[15] S. Tourneur,[15] W. Trischuk,[32] R. Tsuchiya,[56] S. Tsuno,[39] D. Tsybychev,[16] N. Turini,[44] F. Ukegawa,[54] T. Unverhau,[19] S. Uozumi,[54] D. Usynin,[43] L. Vacavant,[28] A. Vaiciulis,[47] A. Varganov,[33] S. Vejcik III,[15] G. Velev,[15] V. Veszpremi,[46] G. Veramendi,[23] T. Vickey,[23] R. Vidal,[15] I. Vila,[10] R. Vilar,[10] I. Vollrath,[32] I. Volobouev,[28] M. von der Mey,[7] P. Wagner,[51] R.G. Wagner,[2] R.L. Wagner,[15] W. Wagner,[25] R. Wallny,[7] T. Walter,[25] Z. Wan,[50] M.J. Wang,[1] S.M. Wang,[16] A. Warburton,[32] B. Ward,[19] S. Waschke,[19] D. Waters,[30] T. Watts,[50] M. Weber,[28] W.C. Wester III,[15] B. Whitehouse,[55] D. Whiteson,[43] A.B. Wicklund,[2] E. Wicklund,[15] H.H. Williams,[43] P. Wilson,[15] B.L. Winer,[38] P. Wittich,[43] S. Wolbers,[15] C. Wolfe,[12] M. Wolter,[55] M. Worcester,[7] S. Worm,[50] T. Wright,[33] X. Wu,[18] F. Würthwein,[8] A. Wyatt,[30] A. Yagil,[15] T. Yamashita,[39] K. Yamamoto,[40] J. Yamaoka,[50] C. Yang,[59] U.K. Yang,[12] W. Yao,[28] G.P. Yeh,[15] J. Yoh,[15] K. Yorita,[56] T. Yoshida,[40] I. Yu,[27] S. Yu,[43] J.C. Yun,[15] L. Zanello,[49] A. Zanetti,[53] I. Zaw,[20] F. Zetti,[44] J. Zhou,[50] and S. Zucchelli[4]

(CDF Collaboration)

[1]*Institute of Physics, Academia Sinica, Taipei, Taiwan 11529, Republic of China*
[2]*Argonne National Laboratory, Argonne, Illinois 60439*
[3]*Institut de Fisica d'Altes Energies, Universitat Autonoma de Barcelona, E-08193, Bellaterra (Barcelona), Spain*
[4]*Istituto Nazionale di Fisica Nucleare, University of Bologna, I-40127 Bologna, Italy*
[5]*Brandeis University, Waltham, Massachusetts 02254*
[6]*University of California, Davis, Davis, California 95616*
[7]*University of California, Los Angeles, Los Angeles, California 90024*
[8]*University of California, San Diego, La Jolla, California 92093*
[9]*University of California, Santa Barbara, Santa Barbara, California 93106*
[10]*Instituto de Fisica de Cantabria, CSIC-University of Cantabria, 39005 Santander, Spain*
[11]*Carnegie Mellon University, Pittsburgh, PA 15213*
[12]*Enrico Fermi Institute, University of Chicago, Chicago, Illinois 60637*
[13]*Joint Institute for Nuclear Research, RU-141980 Dubna, Russia*
[14]*Duke University, Durham, North Carolina 27708*
[15]*Fermi National Accelerator Laboratory, Batavia, Illinois 60510*
[16]*University of Florida, Gainesville, Florida 32611*
[17]*Laboratori Nazionali di Frascati, Istituto Nazionale di Fisica Nucleare, I-00044 Frascati, Italy*
[18]*University of Geneva, CH-1211 Geneva 4, Switzerland*
[19]*Glasgow University, Glasgow G12 8QQ, United Kingdom*
[20]*Harvard University, Cambridge, Massachusetts 02138*
[21]*Division of High Energy Physics, Department of Physics, University of Helsinki and Helsinki Institute of Physics, FIN-00014, Helsinki, Finland*
[22]*Hiroshima University, Higashi-Hiroshima 724, Japan*
[23]*University of Illinois, Urbana, Illinois 61801*

[24] The Johns Hopkins University, Baltimore, Maryland 21218
[25] Institut für Experimentelle Kernphysik, Universität Karlsruhe, 76128 Karlsruhe, Germany
[26] High Energy Accelerator Research Organization (KEK), Tsukuba, Ibaraki 305, Japan
[27] Center for High Energy Physics: Kyungpook National University, Taegu 702-701; Seoul National University, Seoul 151-742; and SungKyunKwan University, Suwon 440-746; Korea
[28] Ernest Orlando Lawrence Berkeley National Laboratory, Berkeley, California 94720
[29] University of Liverpool, Liverpool L69 7ZE, United Kingdom
[30] University College London, London WC1E 6BT, United Kingdom
[31] Massachusetts Institute of Technology, Cambridge, Massachusetts 02139
[32] Institute of Particle Physics: McGill University, Montréal, Canada H3A 2T8; and University of Toronto, Toronto, Canada M5S 1A7
[33] University of Michigan, Ann Arbor, Michigan 48109
[34] Michigan State University, East Lansing, Michigan 48824
[35] Institution for Theoretical and Experimental Physics, ITEP, Moscow 117259, Russia
[36] University of New Mexico, Albuquerque, New Mexico 87131
[37] Northwestern University, Evanston, Illinois 60208
[38] The Ohio State University, Columbus, Ohio 43210
[39] Okayama University, Okayama 700-8530, Japan
[40] Osaka City University, Osaka 588, Japan
[41] University of Oxford, Oxford OX1 3RH, United Kingdom
[42] University of Padova, Istituto Nazionale di Fisica Nucleare, Sezione di Padova-Trento, I-35131 Padova, Italy
[43] University of Pennsylvania, Philadelphia, Pennsylvania 19104
[44] Istituto Nazionale di Fisica Nucleare Pisa, Universities of Pisa, Siena and Scuola Normale Superiore, I-56127 Pisa, Italy
[45] University of Pittsburgh, Pittsburgh, Pennsylvania 15260
[46] Purdue University, West Lafayette, Indiana 47907
[47] University of Rochester, Rochester, New York 14627
[48] The Rockefeller University, New York, New York 10021
[49] Istituto Nazionale di Fisica Nucleare, Sezione di Roma 1, University di Roma "La Sapienza," I-00185 Roma, Italy
[50] Rutgers University, Piscataway, New Jersey 08855
[51] Texas A&M University, College Station, Texas 77843
[52] Texas Tech University, Lubbock, Texas 79409
[53] Istituto Nazionale di Fisica Nucleare, University of Trieste/ Udine, Italy
[54] University of Tsukuba, Tsukuba, Ibaraki 305, Japan
[55] Tufts University, Medford, Massachusetts 02155
[56] Waseda University, Tokyo 169, Japan
[57] Wayne State University, Detroit, Michigan 48201
[58] University of Wisconsin, Madison, Wisconsin 53706
[59] Yale University, New Haven, Connecticut 06520

(Dated: September 19, 2018)

We present a measurement of the ratio of top-quark branching fractions $R = \mathcal{B}(t \to Wb)/\mathcal{B}(t \to Wq)$, where q can be a b, s or a d quark, using lepton-plus-jets and dilepton data sets with integrated luminosity of $\sim$162 pb^{-1} collected with the Collider Detector at Fermilab during Run II of the Tevatron. The measurement is derived from the relative numbers of $t\bar{t}$ events with different multiplicity of identified secondary vertices. We set a lower limit of $R > 0.61$ at 95% confidence level.

PACS numbers: 14.65.Ha, 12.15.Hh

The top quark as described by the Standard Model (SM) is expected to decay to a W boson and a bottom quark at least 99.8% of the time at 90% confidence level (CL) [1]. The Cabbibo-Kobayashi-Maskawa (CKM) quark-mixing matrix [2, 3] element $|V_{tb}|$ is expected to be very close to unity from the assumption of a unitary, three-generation matrix and the measured small values of $|V_{ub}|$ and $|V_{cb}|$ [1]. A measurement of the ratio of top-quark branching fractions $R = \mathcal{B}(t \to Wb)/\mathcal{B}(t \to Wq)$, where q can be a b, s or a d quark, significantly less than unity would contradict our current theoretical assumptions, implying either non-SM top decay, a non-SM background to top-pair production, or a fourth generation of quarks. A previous measurement has set a lower limit of $R > 0.56$ at 95% CL [4]. In this Letter we present a measurement of R using $t\bar{t}$ events collected at the Collider Detector at Fermilab (CDF) during Run II of the Tevatron, a proton-antiproton collider with center of mass energy of $\sqrt{s} = 1.96$ TeV. The integrated luminosity of the data sample used in this analysis is $\sim$162 pb^{-1}.

Our measurement uses $t\bar{t}$-pair events. The lifetime of top is too short for hadronization to occur, and the SM strongly favors an essentially immediate decay of each quark to a real W boson and weak-isospin -1/2 quark; if $R = 1$, this is always a b quark. To maintain high detection and trigger efficiencies and low background levels, we only consider $t\bar{t}$ final states in which at least one W has decayed leptonically. Events in which one W decays leptonically are called "lepton-plus-jets" (L+J) events, and events with two leptonic decays are called "dilepton" (DIL) events. Values of R are determined separately for each of these sets of events, and are combined in the end to set a lower limit on R. The greater statistical power comes from the L+J sample.

The measurement requires both the counting of b-quark jets and the determination of the $t\bar{t}$ content as a function of the b-quark multiplicity. We identify ("tag") b-quark jets by identifying displaced secondary vertices using the SECVTX algorithm [5]. R is extracted from the relative rates of events with zero, one, and two tags; any two rates determine R uniquely, while all three rates jointly overdetermine R. A novel feature of this measurement is the inclusion of the 0-tag L+J event rate, which is determined using event kinematics and an artificial neural net (ANN) technique. As R depends only on relative rates, this measurement is independent of any assumptions of the overall $t\bar{t}$ cross section. However, our measurement of R does depend critically on the knowledge of the efficiency to identify b jets. To extract R we use the efficiency to tag jets in $t\bar{t}$ events estimated with a Monte Carlo (MC) sample in which tagging efficiencies have been tuned to match jet data [5].

The CDF detector for Run II [6] consists of a charged-particle tracking system in a magnetic field of 1.4 T, segmented electromagnetic and hadronic calorimeters and muon detectors. A silicon microstrip detector provides tracking over the radial range 1.5 to 28 cm, and is essential for the detection of displaced secondary vertices. The fiducial region of the silicon detector covers the pseudo-rapidity range $|\eta| < 2$, while the central tracking system and muon chambers provide coverage for $|\eta| < 1$ [7]. A three-level trigger system is used to select events with electron (muon) candidates with E_T (p_T) > 18 GeV (18 GeV/c), which form the data set for this analysis.

L+J events consist of one isolated high-p_T lepton (e or μ), large missing transverse energy ($\not\!\!E_T$) due to the undetected neutrino, and four hadronic jets. Two of these jets arise from the hadronic decay of the other W, and the other two arise from the top-daughter quarks q. The L+J selection requirements are described in detail elsewhere [5]. Briefly, we require the presence of an isolated lepton which has transverse momentum greater than 20 GeV/c, that $\not\!\!E_T$ is at least 20 GeV, and that there is a minimum of four jets, clustered with a cone-based algorithm having cone dimension $\Delta R = \sqrt{(\Delta\phi)^2 + (\Delta\eta)^2} = 0.4$, within $|\eta| < 2$ and with corrected transverse energy [5] greater than 15 GeV. These requirements select 107 events.

TABLE I: Summary of observed number of events with i tags in the L+J and DIL samples, with estimates of nominal $t\bar{t}$ event-tagging efficiencies, background levels and expected event yields. The L+J 0-tag background is measured with an ANN. The efficiency estimates and the 1-tag and 2-tag L+J background estimates are given for $R = 1$. Equations 1 and 2 are used for the calculation of the expected total number of events $N_i^{\rm exp}$. The statistical and systematic uncertainties have been combined.

Lepton + Jets (L+J)	**0-tag**	**1-tag**	**2-tag**
Efficiency ($\epsilon_i(R=1)$)	0.45 ± 0.03	0.43 ± 0.02	0.12 ± 0.02
Background ($N_i^{\rm bkg}$)	62.4 ± 9.0	4.2 ± 0.7	0.2 ± 0.1
Total expected ($N_i^{\rm exp}$)	80.4 ± 5.2	21.5 ± 4.1	5.0 ± 1.4
Observed ($N_i^{\rm obs}$)	79	23	5
Dileptons (DIL)	**0-tag**	**1-tag**	**2-tag**
Efficiency ($\epsilon_i(R=1)$)	0.47 ± 0.03	0.43 ± 0.02	0.10 ± 0.02
Background ($N_i^{\rm bkg}$)	2.0 ± 0.6	0.2 ± 0.1	< 0.01
Total expected ($N_i^{\rm exp}$)	6.1 ± 0.4	4.0 ± 0.2	0.9 ± 0.2
Observed ($N_i^{\rm obs}$)	5	4	2

DIL events consist of two charged leptons (ee, $\mu\mu$ or $e\mu$), large $\not\!\!E_T$ due to the undetected neutrinos, and two jets from the top-daughter quarks q. The DIL selection requirements are described in detail elsewhere [8]. Compared to the L+J selection, we demand an additional lepton, but only a minimum of two energy-corrected [8] jets, with the same requirements as before. These requirements select 11 events.

Both event samples are subdivided on the basis of the number of identified b jets in the event. The number of events in each subsample with i tagged jets are given in Table I. The 2-tag subsample is defined to include events with ≥ 2 tags; in this data sample we observe no events with more than two tagged jets.

In the L+J sample, the dominant background is W production in association with jets from QCD processes ("W+jets" events). In the 1-tag and 2-tag subsamples we make an *a priori* estimate of the backgrounds with a collection of data-driven and simulation techniques that are described in detail elsewhere [5]. The backgrounds in these subsamples include W production in association with heavy-flavor jets ($Wb\bar{b}$, $Wc\bar{c}$, Wc), W production in association with light-flavor jets that are incorrectly identified as b jets ("mistags"), QCD multi-jet ("QCD") events containing fake or real leptons and/or incorrectly-measured $\not\!\!E_T$, dibosons (WW, WZ) and single-top quark production. The background estimate requires a small correction for $R \neq 1$. The background estimate for $R = 1$ in these subsamples is given in Table I. The uncertainties on the estimate are dominated by uncertainties in the fraction of W+jets events that include heavy flavor and on the normalization of the QCD background rate.

By construction, the *a priori* method cannot predict the background level in the 0-tag L+J sample,

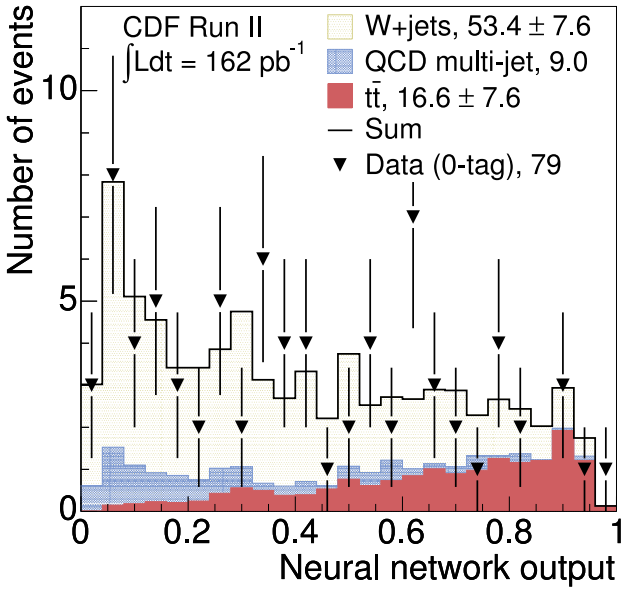

FIG. 1: Fit of the ANN output in the 0-tag L+J data set (triangles) with a sum of 3 components: W+jets (upper), QCD multi-jet (middle), and $t\bar{t}$ (lower). The QCD normalization is independently estimated and not varied in the fit; its shape is determined from the non-isolated lepton data.

where the W+jets production rate dominates that for $t\bar{t}$ pairs; instead we make use of event kinematics [9]. The artificial neural net [10] is trained with the $t\bar{t}$ signal (HERWIG [11]) and W+jets background (HERWIG+ALPGEN [12]) events simulated with a detailed detector description based on GEANT [13]. There is an additional QCD background which is modeled using data with non-isolated leptons. We find optimal signal to background discrimination with an ANN structure of nine input variables, one intermediate layer with ten nodes, and one output unit. The variables used are the transverse energies of the four leading jets, the minimum di-jet mass, the di-jet transverse mass with value closest to the mass of the W, the scalar sum of the transverse energies of all leptons and jets, the total longitudinal momentum divided by the total transverse momentum, and the event aplanarity.

The ANN output ranges from zero for background-like events to one for signal-like events. We perform a binned maximum likelihood fit of the ANN output distribution for the $t\bar{t}$ fraction in the 0-tag subsample. The fraction of events from QCD backgrounds is fixed to 11.4% in this fit. These events are characterized by the non-isolation of the lepton and small $\not\!\!E_T$, and the fixed rate is based on comparing to control regions with either low $\not\!\!E_T$ or poor isolation [5]. The resulting measurement of background rates in the 0-tag L+J subsample is given in Table I. The fit of the distribution of ANN outputs for this subsample is shown in Figure 1.

Systematic uncertainties in the ANN-determined backgrounds are dominated by our understanding of the jet energy scale, the renormalization and factorization scale, and the shape of the QCD template and are strongly anti-correlated between the $t\bar{t}$ and W+jets measurements. Our ANN-measured $t\bar{t}$ content in the L+J sample without any tagging requirement is consistent with that found in our earlier measurement of the $t\bar{t}$ production cross section [14]. The procedure is repeated in the 1-tag and 2-tag samples, yielding background rates of 5.8 ± 5.2 and $0.1^{+1.0}_{-0.1}$ respectively, consistent with the *a priori* estimates shown in Table I. As the *a priori* estimates have smaller uncertainties in the 1-tag and 2-tag subsamples, the ANN-determined background level is used only for the L+J 0-tag subsample.

The main backgrounds in the DIL sample are Drell-Yan production including lepton pairs from the Z resonance, dibosons, and W+jets events with fake leptons. The total background level of 2.2 ± 0.6 events in the DIL sample has been estimated elsewhere [8]. The Drell-Yan rate in ee and $\mu\mu$ events is estimated using simulated data normalized to the observed rate of Z events in the data. Other electroweak backgrounds are estimated from MC simulations. The fake-lepton background is estimated by multiplying each jet in W plus three or more jet events by a lepton fake rate, measured in complementary jet samples.

Most of the jets in the DIL background events arise from generic QCD radiation. To determine the background distribution across the i-tag subsamples, we apply a parameterization of the probability to tag a generic QCD jet [5], derived from jet-triggered data samples, to the jets in the DIL sample, correcting for the enriched $t\bar{t}$ content of the sample. The resulting estimates are given in Table I; the background in the 2-tag subsample is negligible.

The $t\bar{t}$ event-tagging efficiency ϵ_i, defined as the probability to observe i tags in a $t\bar{t}$ event, depends on the fiducial acceptances for jets that can potentially be tagged, and the efficiencies to tag those jets [9]. Those efficiencies in turn depend on the species of the underlying quark in the jet. The efficiency ϵ_i depends strongly on R, as $R \neq 1$ implies fewer b jets available for tagging, and more light-quark jets available instead. We use the jet acceptances and tagging efficiencies to parameterize $\epsilon_i(R)$. These quantities are estimated with a sample of simulated $t\bar{t}$ events from the PYTHIA [15] generator and CDF detector simulation, and their uncertainties are dominated by our understanding of the control samples of jet data used to calibrate tagging efficiencies in the simulation. The leading determiner of ϵ_i is the efficiency to tag a b jet from the decay $t \to Wb$; $\epsilon_b = 0.44 \pm 0.04$ for b jets falling within the fiducial acceptance and having at least two tracks with silicon information. The ϵ_i values also have small contributions from the efficiencies to tag jets from $W \to cs$ hadronic decays and from additional QCD

radiation in $t\bar{t}$ events. The nominal values of ϵ_i for $R = 1$ are given in Table I. The value of ϵ_0 (ϵ_2) changes by -0.28 (0.09) as R changes from 0.5 to 1.

The expected event yield in each of the three tagged subsets of each of the L+J and DIL samples is

$$N_i^{\rm exp} = N_{\rm inc}^{t\bar{t}} \cdot \epsilon_i(R) + N_i^{\rm bkg}, \qquad (1)$$

where $N_i^{\rm bkg}$ is the number of background events in the i-tag subsample and $N_{\rm inc}^{t\bar{t}}$ is an estimate of the inclusive number of $t\bar{t}$ events in the sample, determined by

$$N_{\rm inc}^{t\bar{t}} = \sum\nolimits_i (N_i^{\rm obs} - N_i^{\rm bkg}), \qquad (2)$$

where $N_i^{\rm obs}$ is the observed number of events in each subsample. In this construction, the measured value of R is independent of any assumption of the overall rate of $t\bar{t}$ production, and is thus sensitive only to the relative numbers of $t\bar{t}$ events with i tags.

The full likelihood is a product of independent likelihoods for the L+J and DIL samples. Each likelihood is a product of Poisson functions comparing $N_i^{\rm obs}$ to $N_i^{\rm exp}$ for each value of i, multiplied by Gaussian functions which incorporate systematic uncertainties in the event-tagging efficiencies and backgrounds, taking into account the correlations across the different subsamples. These include correlations in the event-tagging efficiencies through the single-jet tagging efficiencies; in the common methodology of the *a priori* estimates in the tagged L+J samples; and in the overall normalization of the DIL backgrounds. There are a total of five free parameters in the likelihood to account for these systematic uncertainties.

The resulting likelihood as a function of R is shown in Figure 2, along with the negative logarithm of the likelihood. We find a central value of $R = 1.12^{+0.21}_{-0.19}({\rm stat})^{+0.17}_{-0.13}({\rm syst})$. The dominant systematic uncertainties arise from the uncertainty on the background measurement in the 0-tag L+J sample ($^{+0.14}_{-0.11}$) and from the overall normalization of the tagging efficiencies ($^{+0.09}_{-0.06}$). Taken separately, the two final states of $t\bar{t}$ give consistent results for R; the L+J sample alone yields $R = 1.02^{+0.23+0.21}_{-0.20-0.13}$, and the DIL sample alone yields $R = 1.41^{+0.46+0.17}_{-0.40-0.13}$. These R results are consistent with the SM expectations.

The ratio R can only take on physical values between zero and unity. We use the Feldman-Cousins prescription [16] to set a lower limit on R. We generate ensembles of pseudo-experiments for different input values of R (R_{true}), and vary the input quantities of the analysis, *e.g.* the background estimates, taking correlations into account. Using the likelihood-ratio ordering principle, we find the acceptance intervals as shown in Figure 2. With our measured value of R, we find that $R > 0.61$ at the 95% CL.

Our lower limit on R is the strongest limit on this top-quark branching ratio to date. Within the SM, $R = \frac{|V_{tb}|^2}{|V_{tb}|^2+|V_{ts}|^2+|V_{td}|^2}$, up to phase-space factors. Assuming three generations and the unitarity of the CKM matrix, the denominator is unity, and we estimate $|V_{tb}| > 0.78$ at 95% CL. All of our measurements of R are consistent with the SM expectations.

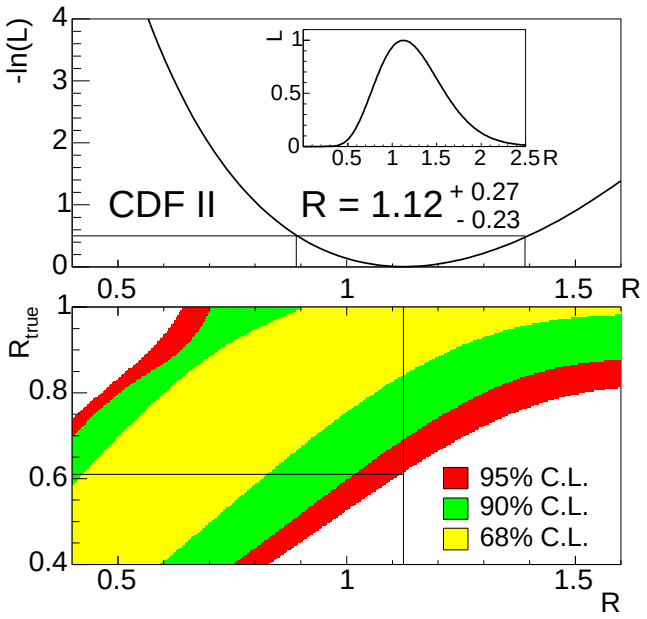

FIG. 2: The upper plot shows the likelihood as a function of R (inset) and its negative logarithm. The intersections of the horizontal line $\ln(L) = -0.5$ with the likelihood define the statistical 1σ errors on R. The lower plot shows 95% (outer), 90% (central), and 68% (inner) CL bands for R_{true} as a function of R. Our measurement of $R = 1.12$ (vertical line) implies $R > 0.61$ at the 95% CL (horizontal line).

We thank the Fermilab staff and the technical staffs of the participating institutions for their vital contributions. This work was supported by the U.S. Department of Energy and National Science Foundation; the Italian Istituto Nazionale di Fisica Nucleare; the Ministry of Education, Culture, Sports, Science and Technology of Japan; the Natural Sciences and Engineering Research Council of Canada; the National Science Council of the Republic of China; the Swiss National Science Foundation; the A.P. Sloan Foundation; the Bundesministerium für Bildung und Forschung, Germany; the Korean Science and Engineering Foundation and the Korean Research Foundation; the Particle Physics and Astronomy Research Council and the Royal Society, UK; the Russian Foundation for Basic Research; the Comision Interministerial de Ciencia y Tecnología, Spain; in part by the European Community's Human Potential Programme under contract HPRN-CT-2002-00292; and the Academy of Finland.

[1] S. Eidelman *et al.* (Particle Data Group), Phys. Lett. B **592**, 1 (2004).

[2] N. Cabibbo, Phys. Rev. Lett. **10**, 531 (1963).

[3] M. Kobayashi and T. Maskawa, Prog. Theor. Phys. **49**, 652 (1973).

[4] T. Affolder *et al.* (CDF Collaboration), Phys. Rev. Lett. **86**, 3233 (2001).

[5] D. Acosta *et al.* (CDF Collaboration), Phys. Rev. D **71**, 052003 (2005).

[6] D. Acosta *et al.* (CDF Collaboration), Tech. Rep. FERMILAB-PUB-04/440-E (2004).

[7] In the CDF geometry, θ is the polar angle with respect to the proton beam axis, and ϕ is the azimuthal angle. The pseudo-rapidity is $\eta \equiv -\ln(\tan(\theta/2))$. The transverse momentum, p_T, is the component of the momentum projected onto the plane perpendicular to the beam axis. The transverse energy E_T of a shower or calorimeter tower is $E \sin\theta$, where E is the energy deposited.

[8] D. Acosta *et al.* (CDF Collaboration), Phys. Rev. Lett. **93**, 142001 (2004), we restrict the 193 pb^{-1} data set used here to runs in which the silicon detector was included.

[9] D. Smirnov, Ph.D. thesis, University of New Mexico (2005).

[10] A. Zell *et al.*, *SNNS: Stuttgart Neural Network Simulator* (2001), user Manual, V4.2. See also `http://www-ra.informatik.uni-tuebingen.de/SNNS/`.

[11] G. Corcella *et al.*, JHEP **01**, 010 (2001), arXiv:hep-ph/0011363.

[12] M. L. Mangano *et al.*, JHEP **07**, 001 (2003), arXiv:hep-ph/0206293.

[13] R. Brun and F. Carminati, CERN Programming Library Long Writeup **W5013** (1993).

[14] D. Acosta *et al.* (CDF Collaboration), submitted to Phys. Rev. D (2005), arXiv:hep-ex/0504053.

[15] T. Sjöstrand *et al.*, Computer Physics Commun. **135**, 238 (2001), arXiv:hep-ph/0108264.

[16] G. Feldman and R. Cousins, Phys. Rev. D **57**, 3873 (1998).